CHEMISTRY OF MATERIALS
Article

Chem. Mater. **2010,** *22,* 5803–5813 5803
DOI:10.1021/cm1007284

Chemical Solution Deposition of Ceria Textured Thin Films from Novel Mixed-Ligand Metal−Organic Precursors

Natalia P. Kuzmina,*,† Sergey A. Ibragimov,§ Artem M. Makarevich,‡ Irina A. Martynova,† Andrey V. Kharchenko,‡ Vladimir V. Korolev,‡ and Sergey V. Kardashov†

†*Department of Chemistry, Moscow State University, Leninskie Gory, 1, bld. 3, 119991, Moscow, Russia,* ‡*Department of Materials Science, Moscow State University, Vorobievy Gory, 1, bld. 3, 119991, Moscow, Russia, and* §*SuperOx Company, Il'inskoe Highway, 9, Arkhangelskoe, Krasnogorskiy District, 143420, Moscow Region, Russia*

Received March 12, 2010. Revised Manuscript Received September 6, 2010

Novel solution precursors for CeO_2 buffer layers, based on mixed-ligand hydroxocomplexes of lanthanide acetates and nitrates with monoethanolamine (MEA) and diglyme, acting as both ligands and solvents, have been developed. The formation of mixed-ligand Ce(IV) complexes in both liquid and transparent gel precursors have been confirmed by electrospray ionization−mass spectroscopy (ESI-MS) and ^{1}H nuclear magnetic resonance (NMR) spectroscopy. The features of thermal decomposition of gel precursor samples were studied using thermogravimetry (TG) and differential thermogravimetry (DTG) analyses in air and in argon. The advantages of the new precursors are the accessibility of high concentrations, stability, and excellent wetting behavior of Ni−5 at.% W substrates. Various elements can be easily incorporated into them as dopants, as was shown on an example of La^{3+}. Epitaxial CeO_2 and CeO_2(La) films were deposited on Ni−W cube-textured tapes from developed solutions via the metal-organic chemical solution deposition (MOCSD) method. Incorporation of La^{3+} into the buffer layer leads to improvement in the oxide's texture and the film's surface.

1. Introduction

During the past few years, efforts have been strongly focused on the development of high-temperature superconducting (HTS) materials based on $YBa_2Cu_3O_{7-x}$ (YBCO) as second-generation HTS (2G HTSC) tapes for electric power applications such as motors, generators, transformers, fault current limiters, magnets, and cables.[1] Such conductors generally represent lengthy epitaxial heterostructures consisting of YBCO films grown on a flexible metallic substrate with intermediate buffer layers and a protection cap layer.[2] The buffer layers play a crucial part in epitaxial heterostructures of 2G HTSC tapes. They act as chemical barriers between the YBCO layer and the substrate, preventing metal-ion diffusion from the substrate into YBCO. Buffers also prevent oxidation of the metallic surface during YBCO film deposition. Because of the percolative nature of the superconducting current, a sharp texture exhibiting only low-angle grain boundaries is essential to obtain high critical current density (J_c) value.[3] Therefore, buffer layers must act as either textured templates or texture transfer layers between the substrate and the YBCO. The most successful buffer layers reported so far are CeO_2, Y_2O_3-stabilized ZrO_2 (YSZ), Y_2O_3, MgO, and $La_2Zr_2O_7$ (LZO).[4−6] The production costs must be as low as possible for the 2G HTSC technology to be economically viable. The technique used to manufacture the buffer and YBCO thin films will play a crucial role in achieving this goal.

Buffer and YBCO layers can be prepared using several deposition methods, which can be divided into two major groups: physical deposition techniques (pulsed laser deposition, sputtering, thermal and e-beam evaporation) and chemical deposition techniques (such as chemical vapor deposition (CVD) and chemical solution deposition (CSD)).[1]

CSD is widely considered to be the most promising route to the low-cost commercial production of HTSC wires, because of its advantages, which include inexpensive nonvacuum equipment, precise control of metal element stoichiometry in the layer, ease of compositional modification on a molecular level, and high deposition rates on large areas. Furthermore, deposition techniques

*Author to whom correspondence should be addressed. Fax: +7 495 939 0998. E-mail address: kuzmina@inorg.chem.msu.ru.

(1) Goyal, A. *Second-Generation HTS Conductors*; Kluwer Academic Publishers: Norwell, MA, 2005.
(2) Foltyn, S. R.; Civale1, L.; MacManus-Driscoll, J. L.; Jia1, Q. X.; Maiorov, B.; Wang, H.; Maley, M. *Nature* **2007**, *6*, 631.
(3) Norton, D. P. *Annu. Rev. Mater. Sci.* **1998**, *28*, 299.
(4) Chirayil, T. G.; Paranthaman, D. B.; Beach, D. B.; Lee, D. F.; Goyal, A.; Williams, R. K.; Cui, X.; Kroeger, D. M.; Feenstra, R.; Verebelyi, D. T.; Christen, D. K. *Physica C* **2000**, 63.
(5) Knoth, K.; Huhne, R.; Oswald, S.; Schultz, L.; Holzapfel, B. *Acta Mater.* **2007**, *55*, 517.
(6) Bhuiyan, M. S.; Paranthaman, M.; Salama, K. *Supercond. Sci. Technol.* **2006**, *19*, R1.

Published on Web 10/14/2010

such as dip coating, drain coating, spray coating, and printing methods allow scalability. An extensive overview about the basics of the chemical solution deposition approach, as well as examples of the growth of oxide films for applications in the semiconductors industry, are discussed in an excellent review by Schwarz.[7] Advantages and disadvantages of the CSD method used for the fabrication of buffer and YBCO layers for 2G HTSC tapes are discussed in various publications.[8]

The CSD method can be generally subdivided into three main stages:[7] (1) *precursor solution synthesis*, which is based on the designated layer composition and the chemical process used; (2) *coating procedure*, which is performed to obtain homogeneous precursor layers of controlled thickness; and (3) *thermal treatment of the precursor layer*, which converts the as-deposited layer to a final crystalline oxide layer via an amorphous state. Each of these stages has a very strong influence on the deposition process. Therefore, the starting compound, as well as the chemical route, should be thoroughly considered.

The wide range of CSD routes can be divided mainly into two classes: the classical sol−gel process and the metal−organic decomposition (MOD) process.[7] Sol−gel processes commonly start from metal alkoxides undergoing hydrolysis and condensation reactions, leading to a colloidal solution (called a sol), and finally to the formation of a three-dimensional gel network. MOD processes are based on metal−organic starting compounds that are insensitive to hydrolysis, such as carboxylates or β-diketonates, which are decomposed during pyrolysis after evaporating the solvents from the as-deposited layer (physical gelation). In our opinion, the MOD approach is a more flexible method for the design and modification of starting metal−organic compounds, because of the possibility of combining metal ions with various organic and inorganic ligands.

In this paper, we present a novel approach to the MOD process. We use organic compounds which act simultaneously as solvents and as ligands. In this case, metal−organic precursors can be described as mixed-ligand complexes with the general simplified formula [ML′L″-(Solv)], where M^{n+} is the desired cation, L′ is an anionic ligand, L″ is a neutral ligand, and Solv represents solvent molecules. Monoethanoleamine (MEA) and diglyme can serve as chelating or bridging O, N ligands, as well as being good solvents for CSD[9] and for wet metal−organic chemical vapor deposition (MO CVD).[10]

Here, we demonstrate the advantages of such approach on an example of deposition of CeO_2 buffer layers on textured Ni−W alloy tape (rolling-assisted biaxially textured substrates, RABiTS), which is a widely used substrate for the production of 2G HTSC wires.[1] CeO_2 is considered to be one of the best buffers for YBCO deposition, because of its excellent chemical compatibility with nickel-based alloy substrates, as well as its good lattice match with YBCO.[11] The admixture of Ln_2O_3 to the CeO_2 layer increases the amount of vacancies and defects, because of the difference in valence between Ln and Ce. Therefore, the CeO_2 layer becomes more flexible, and more subject to further epitaxy formation.[12,13] In the present work, we compare CeO_2 buffer layers doped with La_2O_3 oxide to layers based on pure CeO_2.

2. Experiment

2.1. Precursor Solution Synthesis: Materials and General Procedures. The starting materials $Ce(NO_3)_3 \cdot 6H_2O$, $La(NO_3)_3 \cdot 6H_2O$, acetic acid (HAcet), monoethanolamine (MEA), bis(2-methoxyethyl) ether (diglyme), and acetonitrile (MeCN) of analytically pure grade were purchased from Aldrich. All operations were carried out under atmospheric conditions.

Cerium(III) acetate (denoted as $Ce(Acet)_3 \cdot 2HAcet$) was synthesized according to published procedures.[14] The cerium content was determined via gravimetric analysis: Ce concentration: found, 32.0%; calculated, 32.04%; $\mu_{eff} = 2.4\,\mu_B$.

$La(Acet)_3 \cdot {}^2/_3HAcet$ was synthesized similarly to cerium(III) acetate. A combination of 2.0293 g of $La(NO_3)_3 \cdot 6H_2O$, 10 mL of CH_3COOH, and 30 mL of acetic anhydride were mixed in a round-bottomed flask. The nitric salt was dissolved immediately. The resulting solution then was refluxed with a condenser until the evaporation of brown gas ceased. Precipitation of a white powder was observed as soon as refluxing started. The reaction mixture was cooled to room temperature, and a white powder was filtered and dried under vacuum. The lanthanum content in the carboxylate was determined via titrimetric analysis (yield): La concentration: found, 38.5%; calculated, 39.01%.

2.1.1. Preparation of Test Solutions and Gel Samples. Clear yellowish test solutions were obtained when the starting lanthanide compounds—$Ce(Acet)_3 \cdot 2HAcet$ (3 mmol) or the mixture of $Ce(NO_3)_3 \cdot 6H_2O$ (3 mmol) and HAcet (9 mmol)—were dissolved in MeCN (10 mL) under stirring, followed by the slow addition of 15 or 30 mmol of MEA or/and 15 mmol of diglyme. Compositions of test solutions are presented in Table 1. Numerical coefficients correspond to the molar portions of the reagents.

Test solutions were subjected to thermal treatment to form the gel samples. During the first stage, test solutions were heated at 70 °C for 30 min in air. During the second stage the gels from the first stage were subjected to thermal treatment at 120 °C for 60 min under low pressure

(7) Schwartz, R. W.; Schneller, T.; Waser, R. *C. R. Chim.* **2004**, *7*, 433.
(8) See for example review: Knoth, K.; Engel, S.; Apetrii, C.; Falter, M.; Schlobach, B.; Huhne, R.; Oswald, S.; Schultz, L.; Holzapfel, B. *Curr. Opin. Solid State Mater. Sci.* **2006**, *10*, 205.
(9) Dutta, M.; Mridha, S.; Basak, D. *Appl. Surf. Sci.* **2008**, *254*, 2743.
(10) Molodyk, A. A.; Kaul., A. R.; Gorbenko, O. Yu.; Novozhilov, M. A.; Korsakov, I. E.; Wahl, G. *J. Phys. IV France* **1999**, *9*, Pr8–709.
(11) Bhuiyan, M. S.; Paranthaman, M.; Sathyamurthy, S.; Aytug, T.; Kang, S.; Lee, D. F.; Goyal, A.; Payzant, E. A.; Salama, K. *Supercond. Sci. Technol.* **2003**, *16*, 1305.
(12) Graboy, I. E.; Markov, N. V.; Maleev, V. V.; Kaul, A. R.; Polyakov, S. N.; Svetchnikov, V. L. *J. Alloys Compd.* **1997**, *251*, 318.
(13) Coll, M.; Gazquez, J.; Huhne, R.; Holzapfel, B.; Morilla., Y.; Garcıa-Lopez, J.; Pomar, A.; Sandiumenge, F.; Puig, T.; Obradors, X. *J. Mater. Res.* **2009**, *24*, 1446.
(14) Hay, N. E.; Kochi, J. K. *J. Inorg. Nucl. Chem.* **1968**, *30*, 884.

Table 1. Composition of Test Solutions and Set of Gel Conventional Signs

solution	test solution composition	gel conventional sign[a]
No. 1	$1Ce(NO_3)_3 \cdot 6H_2O-3HAcet-5MEA$	Gel1-70, Gel1-120
No. 2	$1Ce(NO_3)_3 \cdot 6H_2O-3HAcet-10MEA$	Gel2-120
No. 3	$1La(NO_3)_3 \cdot 6H_2O-3HAcet-5MEA$	Gel3-70, Gel3-120
No. 4	$1Ce(Acet)_3 \cdot 2Hacet-5MEA$	Gel4-120
No. 5	$1Ce(Acet)_3 \cdot 2Hacet-10MEA$	Gel5-120
No. 6	$1Ce(Acet)_3 \cdot 2Hacet-5diglyme-5MEA$	Gel6-120
No. 7	$1Ce(NO_3)_3 \cdot 6H_2O-3HAcet-5MEA-5diglyme$	Gel7-70, Gel7-120
No. 8	$0.9Ce(NO_3)_3 \cdot 6H_2O-0.1La(NO_3)_3 \cdot 6H_2O-3HAcet-5MEA-5diglyme$	Gel8-120
No. 9	$0.9Ce(Acet)_3 \cdot 2Hacet-0.1La(Acet)_3 \cdot Hacet-5diglyme-5MEA$	Gel9-120

[a] In conventional sign procedure, the first figure represents the test solution number and the second value shows the temperature of thermal treatment.

Table 2. Major Ions Observed in the ESI+ Spectra of Test Solutions

test solution	major ions observed (m/z)
No. 1	$[Ce(NO_3)(OH)_2(H_2O)_2(MEA)]^+$ (332), $[Ce(OH)_2(Acet)(H_2O)_4]^+$ (304), $[Ce(Acet)(OH)_2(H_2O)_3(MEA)]^+$ (347), $[Ce(OH)_3(H_2O)_2(MEA)]^+$ (288)
No. 2	$[Ce(NO_3)(OH)_2(H_2O)_2(MEA)]^+$ (332), $[Ce(OH)_2(Acet)(H_2O)_4]^+$ (304), $[Ce(Acet)(OH)_2(H_2O)_3(MEA)]^+$ (347), $[Ce(OH)_3(H_2O)_2(MEA)]^+$ (288)
No. 4	$[Ce(OH)_3(H_2O)_2]^+$ (227), $[Ce(OH)_3(H_2O)_2(MEA)]^+$ (288), $[Ce(MEA)_2(OH)_3(H_2O)_3]^+$ (368), $[Ce(OH)_3(H_2O)_3]^+$ (244)
No. 5	$[Ce(OH)(MEA\text{-}H)_2]^+$ (277), $[Ce(OH)_3(H_2O)_2]^+$ (227), $[Ce(OH)_3(H_2O)_3]^+$ (24), $[Ce(OH)_3(H_2O)_2(MEA)]^+$ (288), $[Ce(MEA)_2(OH)_3(H_2O)_3]^+$ (368)
No. 6	$[Ce(Acet)_2(OH)(H_2O)_2(MEA)]^+$ (354), $[Ce(OH)_3(diglyme)]^+$ (325)
No. 7	$[Ce(NO_3)(diglyme)(OH)_2(H_2O)_2]^+$ (404), $[Ce(MEA)_2(OH)_3(H_2O)_3]^+$ (368), $[Ce(OH)_3(diglyme)]^+$ (325), $[Ce(NO_3)(Acet)(OH)(H_2O)]^+$ (296), $[Ce(OH)_3(H_2O)_2]^+$ (227)

Table 3. ^{1}H NMR Data for MEA, Diglyme, and Gel Samples (d^6-DMSO−CCl_4/TMS)

	Chemical Shift (ppm)					
	$Acet^-$	MEA			Diglyme	
sample	CH_3	$-CH_2NH_2 + -OH$	$-CH_2- + H_2O_{DMSO}$	$H_2O + OH^-$	$2CH_3-$	$2 -CH_2CH_2-$
MEA		2.59tr (5H)	3.37tr (5H)			
MEA-70		2.57tr (5H)	3.37tr (4H)			
diglyme					3.28s (6H)	3.42−3.45q, 3.50−3.53q (8H)
GEL1-70	1.79 (3H)	2.64tr (60H, 12MEA)	3.39tr (120H)	4.67, 6.13 (220H, 19H)		
GEL1-120	1.77 (3H)	2.85tr (99H, 20MEA)	3.56tr (40H)	5.11, 7.78 (52H, 152H)		
GEL2-120	1.79 (3H)	2.86tr (104H, 21MEA)	3.54 (48H)	5.30, 7.52 (44H, 123H)		
GEL3-70	1.72 (3H)	2.77tr (20H, 4MEA)	3.51tr (20H)	5.71 (44H).		
GEL3-120	1.72 (3H)	2.65tr (212H, 42MEA)	3.42tr (120H)	4.03 (44H)		
GEL4-120	1.71 (3H)	2.72tr (71H, 14MEA)	3.47tr (54H)	5.50 (142H)		
GEL5-120	1.71 (3H)	2.74tr (75H, 15MEA)	3.48tr (75H)	5.50 (145H)		
GEL6-120	1.81 (3H)	2.86tr (170H, 34MEA)	3.60tr (152H)	4.59 (667H)	3.33s (6H, 1diglyme)	3.40q, 3.54q (8 H)
GEL7-70	1.86 (3H)	2.86tr (50H, 10MEA)	3.40tr (30H)	3.74 (108H)	3.32 (56H, 9 diglyme)	3.46q, 3.54q (72H)
GEL7-120	1.85 (3H)	2.84tr (65H, 13 MEA)	3.38tr (41H)	3.98 (162H)	3.31 (6H, 1 diglyme)	3.46q, 3.55q (9H)

(∼0.1 Torr). The composition of test solutions and set of conventional signs of gel samples, which were studied by appropriate methods, are given in Table 1. The lanthanum-containing solutions and gels (see Table 1, solution No. 3, No. 8, and No. 9) were prepared by analogy with corresponding cerium samples.

2.1.2. Characterization of Test Solutions and Gel Samples. The mass spectra of cerium-containing solutions were recorded on an Agilent LC/MSD 1100 SL mass spectrometer (electrospray ionization at atmospheric pressure, positive-ion mode, ion trap mass analyzer, solution flow rate of 10 μL/min, drying gas (N_2) temperature of 120 °C, nebullizer voltage of 5500 V, capillary voltage of 0−300 V). The major ions observed in the spectra are listed in Table 2. Since lanthanum has only one isotope, the mass spectra of the La-containing solutions (No. 3, as well as No. 8 and No. 9, containing a 0.1 molar portion of lanthanum) were not recorded.

^{1}H NMR spectra of some gel samples were recorded on a Bruker Model AC-600P spectrometer (analytical frequency = 600 MHz) in d^6-DMSO−CCl_4 (1:1)/TMS (see Table 3). ^{1}H NMR spectra of the starting reagents (diglyme and MEA, as well as MEA subjected to heating at 70 °C in air (MEA-70)) also were recorded in d^6-DMSO−CCl_4 solvent (see Table 3). The d^6-DMSO−CCl_4 solvent had some water in it, which resulted in the appearance of an additional signal in the spectra: δ ppm: 2.51s (6H), 3.33s (1H, H_2O).

Thermal analysis of the gel samples was performed using a Perkin−Elmer Model TGA7 thermogravimetric analyzer in argon and air, at a heating rate of 10 °C/min.

2.1.3. Preparation of the Precursor Solution: General Procedure. The starting lanthanide compounds—$Ln(Acet)_3 \cdot n$HAcet or a mixture of $Ln(NO_3) \cdot nH_2O$ and HAcet (molar ratio = 1:3)—were dissolved in MEA under stirring and mild heating (60 °C) and then the

Table 4. Precursor Solution Composition and Characteristics

solution	composition	concentration (M)	viscosity (mPa/s)
No. 1	$Ce(NO_3)_3 \cdot 6H_2O$ + 3HAcet + MEA-diglyme (1:3)	0.2	18
No. 2	$0.9Ce(Acet)_3 \cdot 2Hacet - 0.1La(Acet)_3 \cdot Hacet$ + MEA-diglyme (1:3)	0.1	12

corresponding volume of diglyme was added slowly. After mixing of all of the components, the precursor solution was heated at 70 °C for 15 min, to obtain a stable yellow-colored solution.

The concentration of prepared solutions ranged from 0.05 M to 0.4 M. The data of preliminary deposition experiments have shown that the optimum concentration lies in the range of 0.1−0.2 M. Therefore, in this paper, we present a study of thin films deposited using the solutions described in Table 4. The solution preparation was carried out under atmospheric conditions.

2.2.1. Deposition. Biaxially textured Ni−5 at.% W tapes (evico GmbH, Germany) were used as substrates. Tapes were cleaned in acetone and ethanol prior to deposition. Precursor solutions No. 1 and No. 2 (see Table 2) were used for deposition.

All film depositions were carried out on the laboratory device (see Figure 1). A cycled reel-to-reel mechanism was used. The velocity of the tape's transport was 3 mm/s. Solution deposition was conducted in Zone 1. The nickel substrate, covered with a thin layer of the solution, then was undergoing gradient heat treatment in Zone 2. Samples were gradually heated in air by moving from the 100 °C area to the 320 °C area. When the samples moved out of Zone 2, they were cooled to room temperature in Zone 3 and then the cycle was repeated. The deposition process was followed by an annealing step. The number of cycles was 5 and 10 for solutions No. 1 and No. 2, respectively.

2.2.2. Annealing. Annealing was done at low pressure (~5.1 mbar) in a quartz tube furnace under a continuous flow of reducing gas mixture (Ar + 10% H_2), to protect the nickel substrate from oxidation. The heating rate was 17 °C/min, and the dwelling time at 1000 °C was 1 h.

2.2.3. Thin Film Characterization. The thickness and composition of obtained films were estimated by Rutherford backscattering (RBS), using He^+ ions with an energy of 1.5 MeV and field-emission scanning electron microscopy (FESEM/EDX) (Leo Supra 50VP/Oxford Instruments INCA Energy$^+$). The phase composition and crystal structures, as well as out- and in-plane orientations of the films, were studied by X-ray diffraction (XRD), using a Rigaku Model SmartLab diffractometer with Cu Kα radiation and an incident beam Ge (220) × 2 monochromator ($\theta-2\theta$, φ-scanning, and ω-scanning XRD).

The films' surface morphology and roughness were examined by atomic force microscopy (AFM) (NT-MDT NTEGRA Aura). The AFM system was operated in tapping mode; for routine measurements, custom silicon cantilevers (MikroMasch) were used; high-resolution AFM images were obtained using MikroMasch cantilevers with a single-crystal diamond (SCD) tip. All images were taken in air at room temperature.

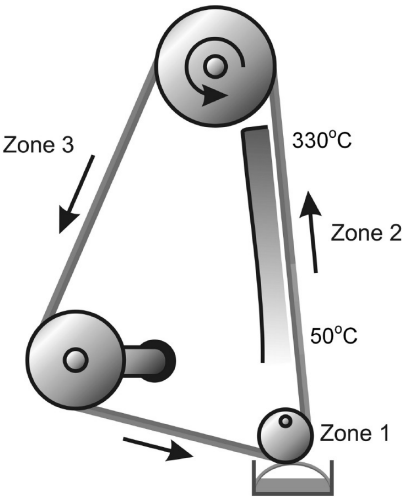

Figure 1. Schematic of a reel-to-reel device used for thin film deposition.

To investigate the surface texture of the films, electron backscatter diffraction (EBSD) was employed (JEOL Model JSM-840A SEM + Oxford Instruments HKL Channel 5).

3. Results and Discussion

3.1. Precursor Characterization. In general, the MOCSD process can be presented as the gradual transformation of a metal−organic precursor (MOP) to oxide thin films:

$$\text{MOP (solution)} \rightarrow \text{MOP (film)} \rightarrow \text{oxide thin film} + \text{by-products} \quad (1)$$

Thorough investigation of every stage shown in expression 1 is necessary to understand and control the oxide thin film deposition process.

Lanthanide carboxylates ($Ln(RCOO)_3$, where R = Me, *i*-Pr, CF_3) are the most popular MOP for CSD preparation of lanthanide-containing oxide thin films.[7,8,15] They decompose with oxide formation at rather low temperature in an oxygen atmosphere (400−700 °C, depending on the nature of the lanthanide). Another advantage of lanthanide carboxylates is their solubility, which can be rather easily adjusted, by varying the R groups in the carboxylate ligand and via the formation of a mixed-ligand coordination compound with different anionic and neutral donor ligands. $Ln(RCOO)_3$ are coordinationally unsaturated compounds, and they are able to include molecules of donor solvents in the coordination sphere of central ions, forming mixed-ligand coordination compounds with high coordination numbers.[16] Therefore, the

(15) Singh, M. K.; Yang, Y.; Takoudisa, C. G. *Coord. Chem. Rev.* **2009**, *253*, 2920.
(16) *Gmelin Hand Book of Inorganic Chemistry*; System No. 39, V. D5; Springer: Berlin/Heidelberg, New York, Tokyo, 1984; 423 pp.

nature of solvent molecules can drastically influence both the MOP solution properties and MOP decomposition.

In this work, the mixed-ligand complex formation approach was used for the modification of cerium(III) acetate as a precursor for the CSD preparation of CeO_2 and $Ce(La)O_2$ buffer layers on cube-textured Ni−W tapes. MEA and diglyme were used as neutral ligands and solvents, in addition to acetate as the main anionic ligand for MOP preparation.

As an aminoalcohol, MEA ($NH_2CH_2CH_2OH$) can potentially act as an O,N-donor ligand to lanthanide ions, because of hydroxyl and amino donor groups. There are only few data that describe lanthanide complexes with MEA and diethanolamine (DEA), which is a well-known analogue of MEA. Replacement reactions between lanthanide isopropoxides and these aminoalcohols are under intense investigation.[17,18] Only hydroxyl hydrogens of MEA and DEA ligands have been reported to be active in such replacement reactions. The reactivity of the hydroxyl groups has been also observed in analogous replacement reactions of anhydrous lanthanide halides, nitrates, and isocyanides with DEA, with the formation of mixed-ligand alkoxide complexes.[19] Based on these data, one might expect that analogous mixed-ligand alkoxides could form by interactions of cerium acetate and nitrate with MEA. Moreover, MEA (which has a viscosity of 17 mPa·s), as well as DEA, have already been successfully used in CSD film deposition processes to increase the viscosity of precursor solution.[9]

Diglyme is a well-known tridentate O-donor molecule. It can act as both a chelating and bridging ligand, with respect to lanthanide ions (for example, in compounds with lanthanide hexafluoroacetylacetonates).[20] There is no literature data concerning mixed-ligand complexes of $Ln(RCOO)_3$ compounds with diglyme. At the same time, diglyme is a commonly used solvent. Moreover, it has been successfully used in the wet MOCVD deposition of YBCO films.[10] Unlike MEA, diglyme has a low viscosity (1.2 mPa·s), and both can be mixed to adjust the viscosity of precursor solutions.

We expected MEA and diglyme to act as both solvents and ligands in MOP preparation. Two cerium compounds—$Ce(Acet)_3 \cdot 2Hacet$ and $Ce(NO_3)_3 \cdot 6H_2O$ mixed with HAcet in a 1:3 molar ratio—were used as starting materials. In the case of MEA, there is a possibility of formation of nitrato-acetato mixed-ligand compounds that can diminish MOP thermal stability. To estimate the chemical composition and behavior of cerium-containing species in precursor solutions, a series of test solutions in MeCN were prepared (see Table 1) and studied by electrospray ionization mass spectrometry (ESI MS).

Mass spectrometry is a powerful technique for identifying metal complexes in solutions. ESI MS is one of the most suitable methods for studying species with ionic or very polar character,[21] especially for paramagnetic species, which cannot be investigated reliably via nuclear magnetic resonance (NMR) spectroscopy, as in the case of Ce(III) compounds.

Test solutions with only diglyme are not stable since a precipitate forms immediately after the admixture of components. However, when the mixture of MEA and diglyme was added to $Ce(Acet)_3 \cdot 2Hacet$ or to the mixture of $Ce(NO_3)_3 \cdot 6H_2O$ with HAcet (as in solutions No. 6, No. 7, No. 8, and No. 9), the solutions remained clear.

The ESI spectra of the test solutions studied (No. 1, No. 2, No. 4, No. 5, No. 6, No. 7) have common features. Based on analysis of the observed m/z values and cerium isotope distribution, the more-representative peaks are assigned to singly charged mononuclear ions of Ce(IV) hydrolyzed species, which contain MEA and acetate or nitrate ligands and diglyme. Because of the strong basic nature of MEA, it should promote the $Ce^{3+/4+}$ oxidation process. Therefore, the addition of MEA to a solution of $Ce(NO_3)_3 \cdot 6H_2O$ (molar ratio 5:1) in MeCN results in the precipitation of cerium(IV) hydroxide. The addition of acetic acid (test solution No. 1) or the use of $Ce(Acet)_3 \cdot 2Hacet$ as the starting compound (test solution No. 4) instead of using pure cerium(III) nitrate leads to the formation of clear solutions. In ESI mass spectra of the latter ones, the peaks of MEA-containing cerium(IV) hydrolyzed species $[Ce(NO_3)(OH)_2(H_2O)_2(MEA)]^+$ and $[Ce(OH)_3(H_2O)_2(MEA)]^+$ are the most intense. The increase in the MEA:Ce molar ratio in solutions (test solutions No. 2 and No. 4) results in a change of spectra character. The signals, corresponding to MEA-containing ions ($[Ce(NO_3)_2(OH)(MEA)_2]^+$ and $[Ce(OH)(MEA-H)_2]^+$, respectively) dominate the spectra. Note that the composition of hydrolyzed species (detected by ESI) spectra can be presented in aminoalcoholate form with the same m/z values, because of the following equilibrium:

$$OH^- + MEA \leftrightarrow H_2O + (MEA-H)^-$$

The signals of mixed-ligand hydrolyzed species of Ce(IV) were detected in the ESI mass spectra of test solutions No. 6 and No. 7: $[Ce(OH)_3(diglyme)]^+$, $[Ce(Acet)_2(H_2O)_2(MEA)]^+$, and $[Ce(NO_3)(diglyme)(OH)_2(H_2O)_2]^+$.

The clear test solutions were transformed to transparent gels via thermal treatment at 70 °C in air and then at 120 °C under low pressure. It is our belief that these operations imitate the formation of as-deposited films on the nickel surface, and it is important to study the chemical composition of these gels and their thermal behavior.

The ^1H NMR spectroscopy method was used to estimate the chemical compositions of the gels, since, according to the ESI MS data, the diamagnetic Ce(IV) species dominate in test solutions. To confirm the oxidation of the Ce(III) starting compounds by interaction with MEA

(17) Sankhia, B. S.; Kapoor, R. N. *Bull. Chem. Soc. Jpn.* **1967**, *40*, 1381.
(18) Gharia, K. S.; Singh, M; Mathur, S.; Sankhla, B. S. *Synt. React. Inorg. Met.-Org. Chem.* **1980**, *10*, 403.
(19) Golub, A. M.; Von Luong, A. *Russ. J. Inorg. Chem.* **1969**, *14*, 702.
(20) Malandrino, G.; Fragala, I. L. *Coord. Chem. Rev.* **2006**, *250*, 1605.
(21) Henderson, W.; Nicholson, B. K.; McCaffray, L. J. *Polyhedron* **1998**, *17*, 4291.

in solutions, ^{1}H NMR spectra of Gel1-70 and Gel1-120 were compared to analogous lanthanum gels (Gel3-70 and Gel3-120). A d_6-DMSO−CCl_4 mixture was chosen as the solvent, because of the insolubility of the gels in other organic solvents. However, this solvent influenced the spectrum of MEA rather significantly. We observed two triplets, at 2.59 and 3.37 ppm, with equal integral intensities, while the literature spectrum of MEA in $CDCl_3$ reveals a triplet at 3.58 ppm and a multiplet at 2.77 ppm, at a respective ratio of 2:5.[22] This change can be explained by chemical interaction of MEA with DMSO and water. Thermal treatment of MEA at 70 °C in air does not affect the spectrum.

In the ^{1}H NMR spectrum of Gel3-70, one singlet (1.72 ppm) originates from the methyl group of the acetic ligand. Two intensive triplet signals, at 2.77 and 3.51 ppm, were ascribed to MEA protons, and the intense signal at 5.71 ppm may be originated from hydroxyl groups and water molecules (see Figure 2b). Based on integral intensity ratios for these signals and the previously reported ESI results, the composition of this gel can be conventionally estimated as $\{La(Acet)_1(MEA)_4(NO_3)_x(OH)_y(H_2O)_z\}$ (i.e., even under light heating, part of the acetic acid is removed from the starting test solution). Further heating results in almost complete (> 90%) removal of the acetic ligand. In the spectrum of Gel3-120, the intensity of methyl proton signal at 1.72 ppm sharply decreases and other signals are still intense and slightly shifted upfield (see Figure 2a). In general, the spectra of the cerium-containing Gel1-70 and Gel1-120 are similar to the spectra of their lanthanum-containing analogues. The same set of signals is present in the spectra; however, some of them are slightly shifted. No significant broadening of the main signals, which would have been caused by Ce(III) species, was observed. The removal of acetic acid from solutions and gels under thermal treatment also was found in the case of test solutions No. 2, No. 4, No. 5, No. 6, and No. 7. Therefore, in the spectra of all Gel-120 samples, the intensities of methyl signals were very low and the signals of MEA, OH, and H_2O were very intense. Also, the character of the spectra was not dependent on the starting cerium compound or the molar portion of MEA in test solutions (the spectra of Gel1-120 and Gel2-120, and the spectra of Gel14-120 and Gel5-120). In the spectra of Gel6-120 and Gel7-120, the signals from diglyme protons also were rather low (see Table 3); this means that the removal of diglyme from gel under heating occurs much faster than the removal of MEA.

Thus, the NMR data shows that the formation of transparent gels from hydrolyzed test solutions is accompanied by removal of the acetic ligand and diglyme; therefore, the gels are composed of mixed-ligand hydroxo species, and they can be described by the general formula

$$Ce(Acet)_a(OH)_x(MEA)_y(MEA-H)_z(H_2O)_q(NO_3)_p(diglyme)_r$$

(22) Spectral Data Base for Organic Compounds. Available via the Internet at http://riodb01.ibase.aist.go.jp/sdbs/cgi-bin/cre_index.cgi.

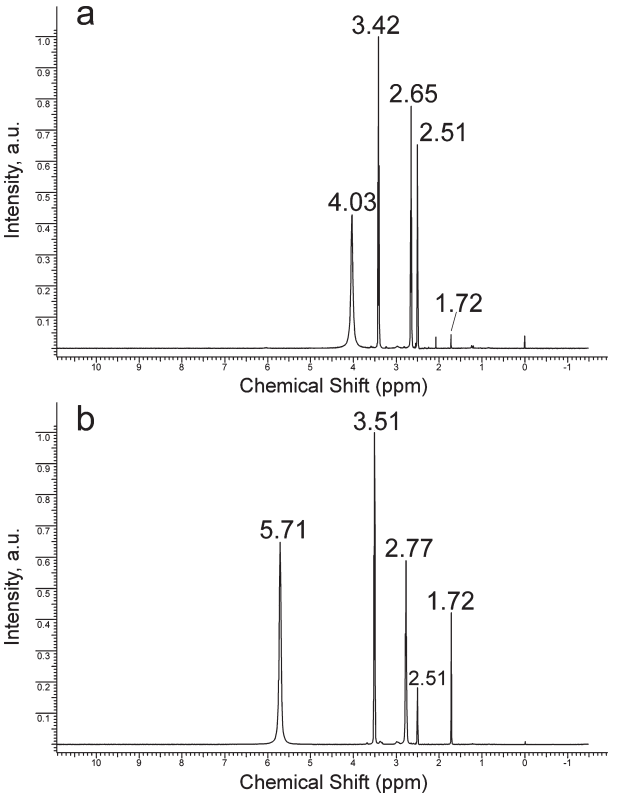

Figure 2. NMR spectra of (a) Gel3-120 and (b) Gel3-70.

where the subscripts *a*, *x*, *y*, *z*, *q*, *p*, and *r* vary, depending on the regime of thermal treatment and composition of the starting precursor solutions. The formation of such mixed-ligand hydroxo species in solutions and in gel samples plays a dominant role in the properties of the new precursors for CeO_2 solution deposition. Furthermore, one would expect that different lanthanides can be easily inserted in such mixed-ligand hydroxo species and, therefore, into the CeO_2 matrix. In this work, we used lanthanum additions (10%), and the corresponding test solutions and gel samples are given in Table 1.

MEA was tested as a solvent, and solutions of both $Ce(Acet)_3 \cdot 2Hacet$ and the $Ce(NO_3)_3 \cdot 6H_2O$-3HAcet mixture with concentrations of > 0.6 M were transparent and stable for months. However, the viscosity of concentrated precursor solutions is rather high and increases with respect to the concentration: from 14 mPa·s for 0.1 M to 32 mPa·s for 0.3 M. Viscosity values of such solutions can be diminished via the addition of solvents with low viscosity; however, solutions that contain several solvents and modifying additives usually could show more complex viscosity behavior. In this work, diglyme was used, in addition to MEA, to diminish the viscosity of the precursor solutions, because it participates in the formation of mixed-ligand hydroxo complexes in the solutions, and finally because of the similarity of boiling points of MEA and diglyme (172 and 167 °C, respectively). A mixture of MEA and diglyme (3:1) was used as a solvent. The viscosities of precursor solutions in this mixed solvent increase as the concentration increases, and they are practically independent of the starting cerium compound ($Ce(Acet)_3 \cdot 2Hacet$ or

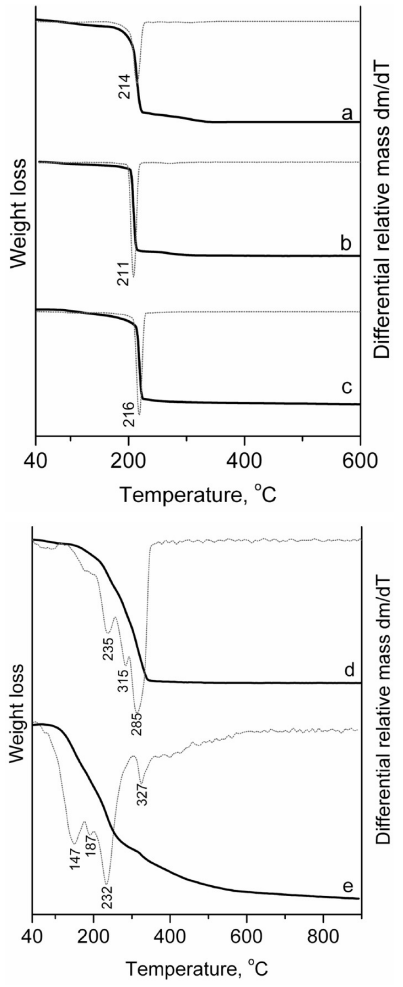

Figure 3. Thermal behavior of (a) Gel2-120 in air, (b) Gel8-120 in air, (c) and Gel8-120 in argon, as well as that of (d) Gel9-120 in air and (e) Gel9-120 in argon.

the mixture $Ce(NO_3)_3 \cdot 6H_2O$-3HAcet). The viscosity values for solutions with concentrations of 0.1 and 0.2 M were equal to 12 and 18 mPa·s. The incorporation of lanthanum does not influence the viscosity values of the precursor solution.

The next step of precursor characterization was thermal analysis of the gel samples, to establish a suitable heat-treatment schedule. The thermal analysis of gel samples was performed in air and in argon (see Figure 3).

The TG curve of Gel2-120 in air shows two stages of weight loss (Figure 3a). The first stage appears in the temperature range of 100−220 °C, with minimums in the DTG curve at 214 °C corresponding to the removal of H_2O, MEA, and acetic acid (~90% of the overall weight loss). The second one is in the range of 220−350 °C (~9%) and is rather smooth. Since >99% of the overall mass loss occurs at these stages below 350 °C, we believe that the thermolysis of this gel sample is almost complete by this temperature. This was confirmed by the XRD data, which showed a formation of CeO_2 in polycrystalline form. The relatively low values of thermolysis temperature in air are in good agreement with the literature data concerning thermal decomposition of Ce(III/IV) nitrates, carboxylates, and hydroxocompounds in air.[23]

The thermolysis of the Gel8-120 sample, which contained a 0.1 molar portion of lanthanum, in addition to cerium (see Table 1)), was of special interest, since it is known that lanthanum compounds (carboxylates, nitrates, and hydroxocompounds) decompose at significantly higher temperatures[16,24,25] than the Ce(III/IV) analogues. Another difference between Gel8-120 and Gel2-120 is that the first one contains diglyme, while the second one does not (see Table 1). The obtained data show that the addition of lanthanum and diglyme practically does not influence the gel thermal behavior. The Gel8-120 sample undergoes two major stages of weight loss upon heating in air (see Figure 3b) in the same temperature range that Gel2-120 does (see Figure 3a). The role of nitrate ions in gel sample thermolysis in air can be seen from a comparison of TG-DTC curves for Gel8-120 and Gel9-120 (see Figures 3b and 3d). The thermolysis of the Gel9-120 sample, which does not contain nitrate ligands, is more complex (four DTG minimums in the range of 100−290 °C) and finishes at a higher temperature (100−550 °C) than that of Gel8-120 (100−350 °C).

In argon, full thermolysis of the Gel8-120 and Gel9-120 samples (see Figures 3c and 3e) occurs in three main stages. These correspond to (1) the removal of water and solvent (MEA and diglyme) molecules, at 100−200 °C; (2) the main thermolysis, in the range of 200−500 °C; and then (3) very slow carbon burning, up to 850 °C. Also note that the thermolysis of nitrate-containing precursors occurs faster and at lower temperatures than the thermolysis of acetate precursors in argon.

Based on these data, the preannealing temperature of films in deposition experiments, carried out in air, was chosen to be 330 °C. The further phase-forming annealing of CeO_2 thin films must be carried out in an inert atmosphere, to prevent the oxidation Ni−5% W tapes. Based on the thermal analysis previously described, we performed these experiments in a $Ar-H_2$ mixture at 1000 °C.

3.2. Thin-Film Characterization. Many deposition experiments were performed with new precursor solutions. They were characterized using XRD, EBSD, RBS, and EDX. Only pure CeO_2 (or La_2O_3-doped CeO_2) was present in all of the deposited films. The advantages of the proposed approach are demonstrated here on two film examples: Film 1, which is a CeO_2 film from solution No. 1, and Film 2, which is La_2O_3-doped CeO_2 from solution No. 2.

3.2.1. Composition and Thickness. Based on EDX and RBS data, Film 1 and Film 2 contained only rare-earth metals (cerium, lanthanum), nickel, tungsten, and oxygen. No detectable amounts of carbon or nitrogen were revealed in these films. This allows us to conclude that no contamination of the films occurred during the deposition and heating processes.

(23) Arii, T.; Kishi, A.; Ogawa, M.; Sawada, Y. *Anal. Sci.* **2001**, *17*, 875.
(24) Wendlandt, W. W. *Anal. Chim. Acta* **1956**, *15*, 435.
(25) Karppinen, V.; Kylakoski, P.; Niinisto, L.; Rodellas, C. *J. Thermal Anal.* **1989**, *35*, 347.

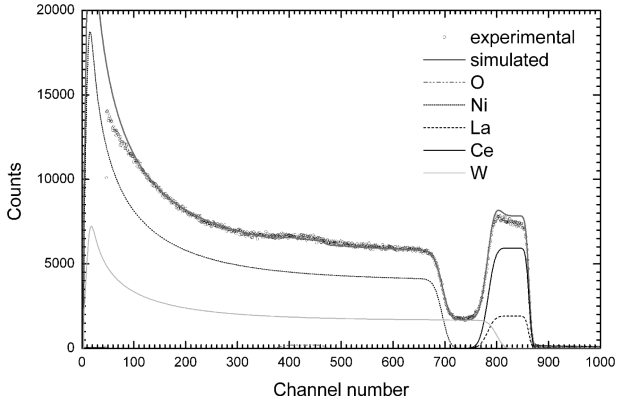

Figure 4. RBS spectra of Film 2.

The oxide layer thickness of Film 2, as estimated from RBS measurements, was 180 nm (see Figure 4). Combining this result and the results of the EDX measurements, the thickness of CeO_2 layers in other films was evaluated. For Film 1, the thickness was estimated to be ~90 nm. The difference in thickness between these two samples can be explained by the different experimental conditions (e.g., the composition and concentration of solutions and the number of deposition cycles).

Both films were one color, except for the small areas (~0.5 mm) near the edges. Taking into account the estimated ceria thickness, the consistency of the color of the film color is pretty strong evidence that both Film 1 and Film 2 are homogeneous. EDX measurements were taken at random points, and the obtained values did not vary.

3.2.2. Texture of the Films. The presence of polycrystalline CeO_2 was already observed on the XRD pattern of thin films after the deposition. This shows that the decomposition of metal−organic complexes with ceria formation already occurs during the heat treatment of our samples in the deposition cycles. After annealing, the ceria films (doped or undoped with La^{3+}) had a pure (00*l*) out-of plane orientation (see Figure 5). Figure 5 displays a typical XRD $\theta-2\theta$ scan for Film 1 and Film 2. The two strong peaks at $2\theta = 32.92°$ (33.1° for Film 1) and 51.5° correspond to CeO_2 (002) and Ni−W (002), respectively, indicating good *c*-axis orientation of the CeO_2 buffer layer in the XRD analysis of both samples. No trace of the CeO_2 (111) peak was identified. The CeO_2 peak is shifted to $2\theta = 32.92°$, because of La^{3+} doping in Film 2. The intensity of the CeO_2 (002) peak is higher in the case of Film 2, which is consistent with the difference in film thickness.

To estimate the in-plane texture and out-of-plane texture in a more precise way, φ-scan and ω-scan rocking curves of both the Ni−W substrate and the CeO_2 single buffer layer were performed. The full width at half maximum (fwhm) of the Ni−W (111) φ-scan was 6.00(1)° and that of the Ni−W (200) ω-scan was also 6.00(1)°.

Both CeO_2 (111) φ-scans show 4-fold symmetry (see Figure 6). In Film 1, the fwhm value is 9.00(1)°, while in Film 2, it is 7.00(1)°. A similar tendency is observed in the fwhm values of CeO_2 (200) ω-scans: 11.00(1)° for Film 1

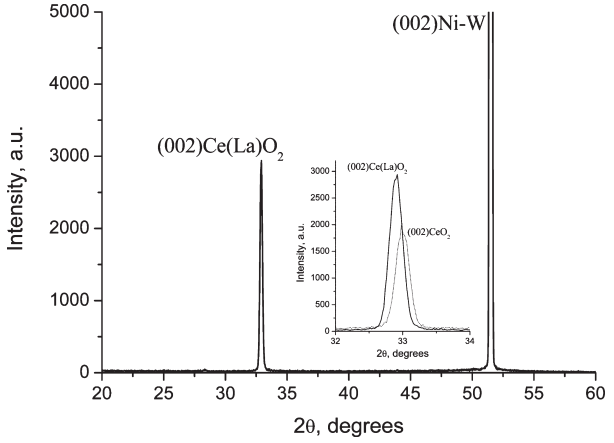

Figure 5. XRD $\theta-2\theta$ pattern of Film 2. The inset depicts the relative intensities of the CeO_2 (001) peaks of Film 1 and Film 2.

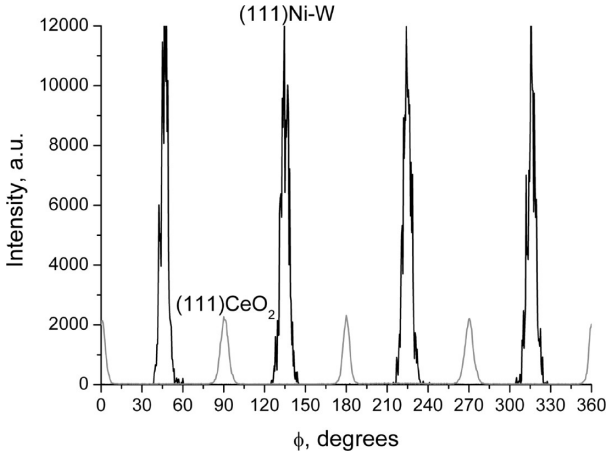

Figure 6. XRD φ-scans of CeO_2 (111) and Ni−W (111) reflections for Film 2.

and 6.00(1)° for Film 2. Epitaxial relations for CeO_2 films on a nickel substrate can be written as (001)[100]‖(001)-[110]. Therefore, La^{3+} doping leads to improved in-plane and out-of-plane texture, which is consistent with the literature data.[13]

3.2.3. Surface of the Films. An EBSD study of the thin surface layer (~10 nm thick) of *c*-axis-oriented Film 1 and Film 2 demonstrates the good crystallinity and sharp in-plane orientation of these layers. Ni−W substrate grain boundaries are reproduced on EBSD maps of CeO_2 films. The average grain size is 20−30 μm, which is consistent with the dimensions of the substrate's grains. Note that La^{3+} doping improves the film's surface (see Figures 7a and 7b). The grain misorientation angle for Film 2 is 5.0(5)°, whereas that for Film 1 is 7.0(5)°. Our results are in good agreement with the literature data.[26]

SEM pictures of Film 1 and Film 2 are shown in Figures 8 and 9, respectively. Both films exhibit grains

(26) See for example: (a) Elmechaouri, M.; Mönter, B.; Krämer, D.; Pusch, H.; Jasper, W.; Erdman, I.; Huehne, R. *J. Phys.: Conf. Ser.* **2008**, *97*, 012042. (b) Hühne, R.; Eickemeyer, J.; Sarma, V. S.; Güth, A.; Thersleff, T.; Freudenberger, J.; Haas, O.; Weigand, M.; Durrell, J. H.; Schultz, L.; Holzapfel, B. *Supercond. Sci. Technol.* **2010**, *23*, 034015. (c) Kotzyba, G.; Obst, B.; Nast, R.; Goldacker, W.; Holzapfel, B. *J. Phys.: Conf. Ser.* **2006**, *43*, 345.

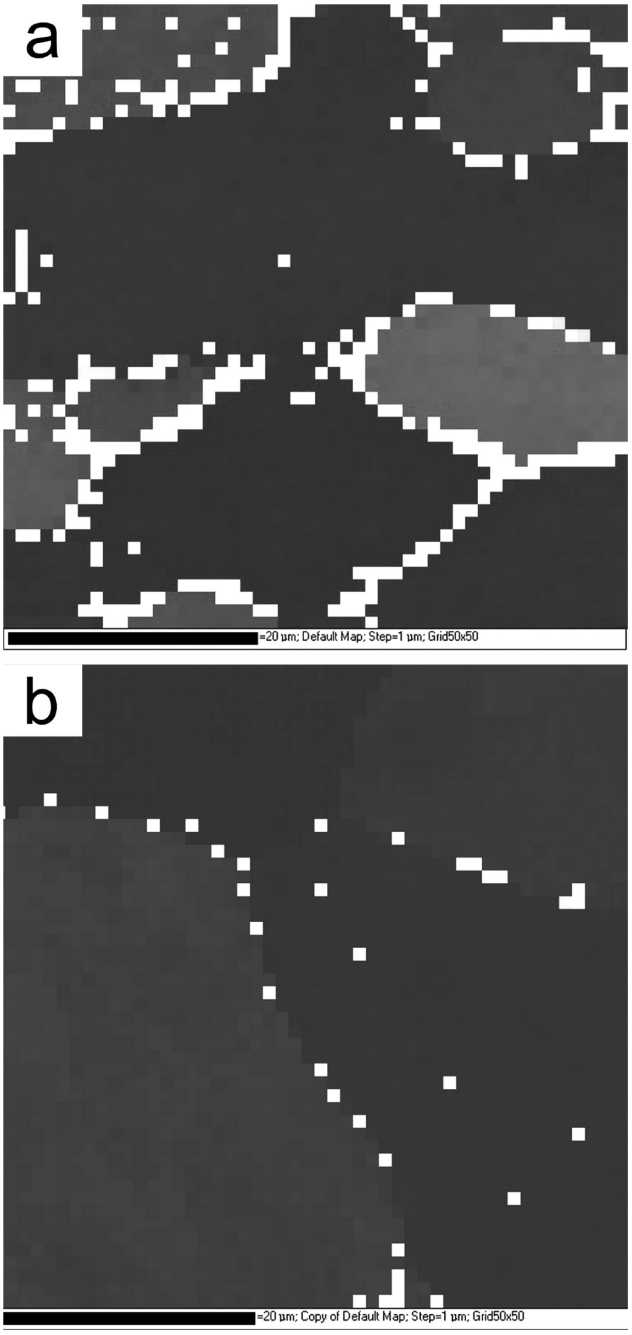

Figure 7. EBSD data (orientation maps) for CeO_2 layers for (a) Film 1 and (b) Film 2.

of the same size, which reproduce the morphology of the nickel substrates. Two regular nets of rectangular cracks are observed on Film 2. They are positioned 45° to each other (see Figure 9). The thicker cracks (Type I), which are in a netlike arrangement, are continuous, parallel, and straight, thus forming rectangles with equal sides of 18.5 μm and 14 μm. The size of these cracks indicates that they originate from regular bendings of the tape during the deposition stage. Their orientation coincides with the orientation of the substrate's lattice. Since CeO_2 grows with 45° rotation on Ni−W tape, these cracks are formed along (100) crystallographic plane of CeO_2.

The thinner cracks in the other set (Type II) also are straight. They form a brick-type motif, where the brick

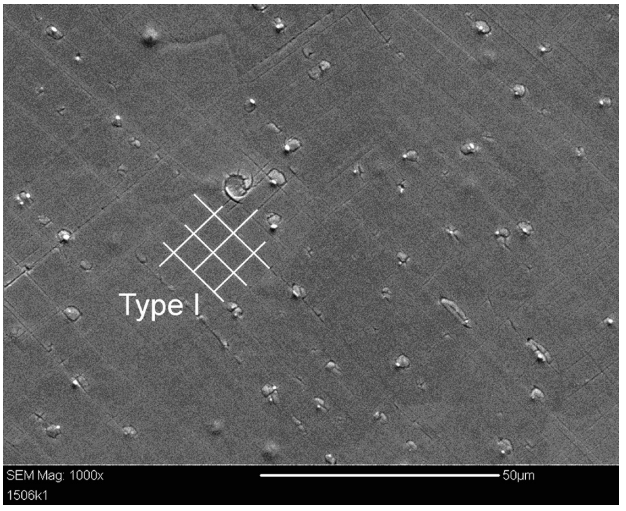

Figure 8. SEM image of Film 1, showing pimples.

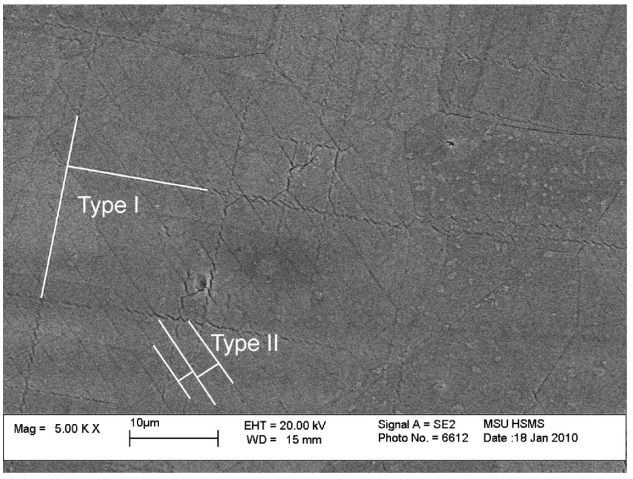

Figure 9. SEM image of Film 2, showing Type I and Type II cracks.

sides are unequal, because of the discontinuous character of the Type II cracks. These cracks are interrupted at an intersection with perpendicular cracks, which leads to uneven rectangles. The size and character of these cracks are similar to defects observed in other works, where a buffer CeO_2 layer was deposited without a reel-to-reel device.[27] Based on the literature data and our judgment, we attribute the origin of these cracks to the different thermal expansion coefficients of the CeO_2 and the nickel substrate. These types of defects are formed along the (110) crystallographic plane of CeO_2. This is expected because, for CeO_2, the surface energy of the (111) plane (5×10^{-5} J/cm^2) and the (110) plane ($(4-7) \times 10^{-5}$ J/cm^2)[28−31] are significantly lower than the surface energy of the (001) plane (1×10^{-4} J/cm^2).[32,33] No other defects are detected on Film 2 via SEM analysis.

(27) See, for example, this review: Bhuiyan, M. S.; Paranthaman, M.; Salama, K. *Supercond. Sci. Technol.* **2006**, *19*, R1.
(28) Tasker, P. W. *J. Phys. Colloq.* **1980**, *41*, C6.
(29) Benson, G. C.; Claxton, T. A. *Can. J. Phys.* **1963**, *41*, 1287.
(30) Tasker, P. W. *J. Phys. C: Solid State Phys.* **1979**, *12*, 4977.
(31) Gilman, J. J. *J. Appl. Phys.* **1960**, *31*, 2208.
(32) Puchin, V. E.; Puchina, A. V.; Huisinga, M.; Reichling, M. *J. Phys.: Condens. Matter* **2001**, *13*, 2081.
(33) Eglitis, R. I.; Shi, H.; Borstel, G. *Surf. Rev. Lett.* **2006**, *13*, 149.

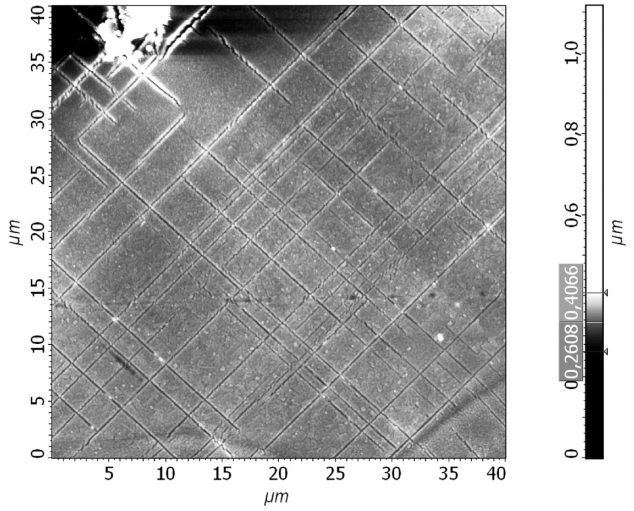

Figure 10. AFM image of Film 1 (dimensions: 40 μm × 40 μm).

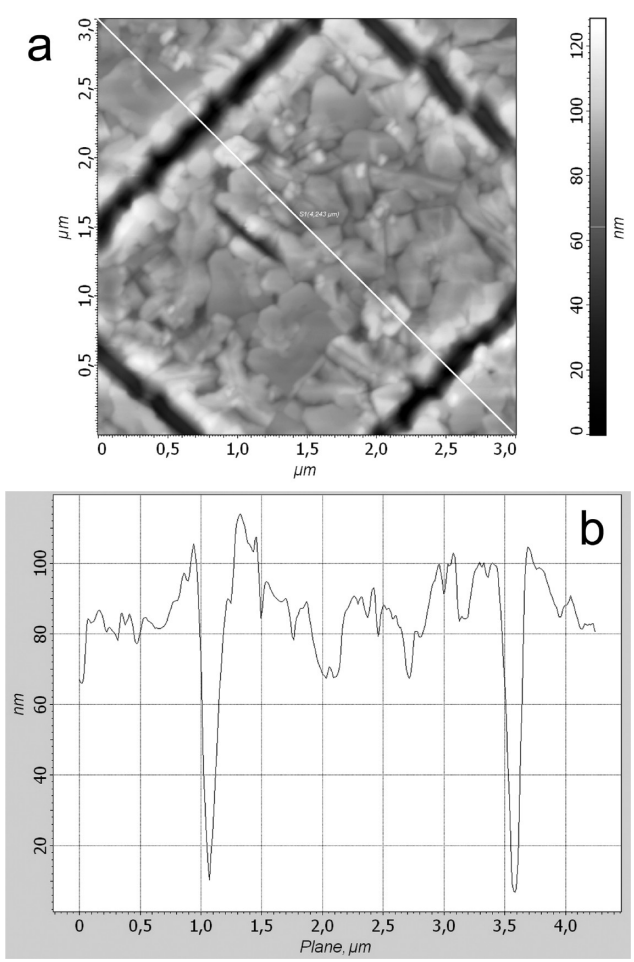

Figure 11. AFM image of Film 1 (dimensions: 3 μm × 3 μm) and section profile of the image along the selected line.

Only Type I cracks, which originate from the bending of the tape during the deposition of the CeO_2 film are observed on Film 1 (see Figure 8). We attribute the absence of Type II cracks in Film 1 to the difference in thickness between Film 1 and Film 2. Since Film 1 is two times thinner than Film 2, it might be more resistant to cracking, as was described by Bhuiyan et al.[27]

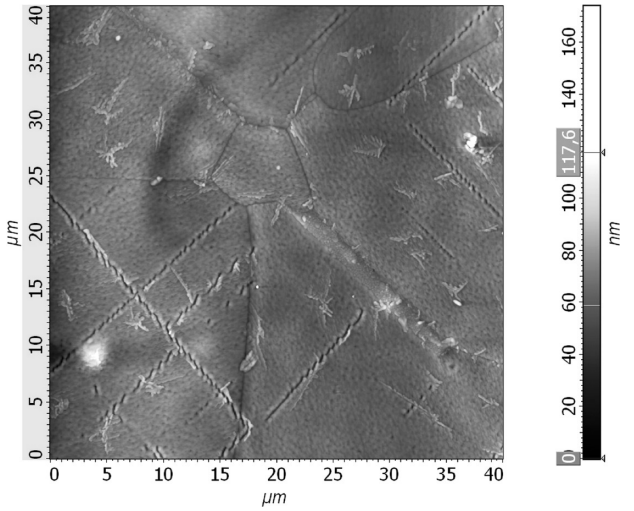

Figure 12. AFM image of Film 2 (dimensions: 40 μm × 40 μm).

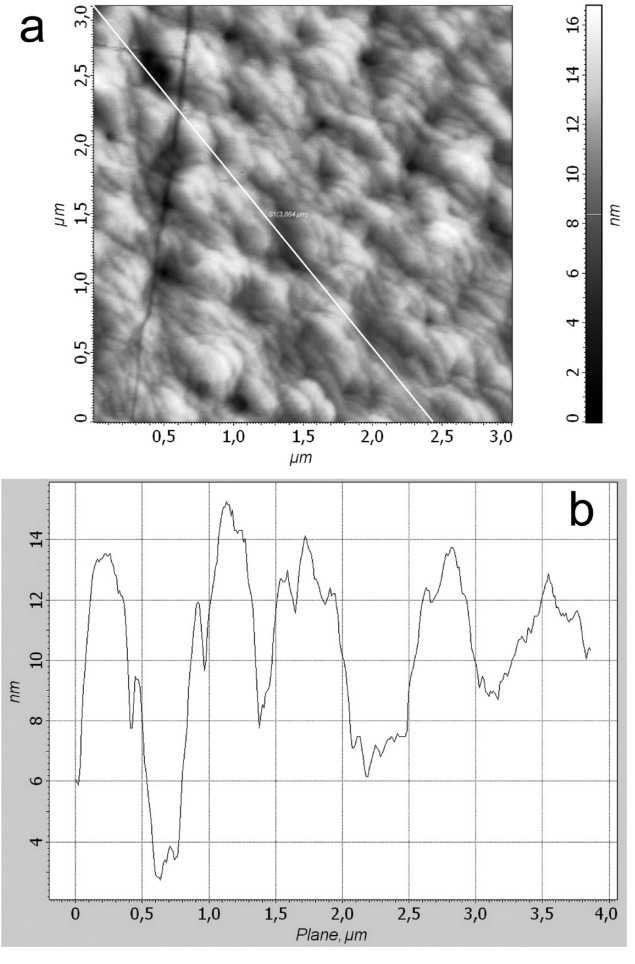

Figure 13. (a) AFM image of Film 2 (dimensions: 3 μm × 3 μm) and (b) section profile of the image along the selected line.

An interesting feature of Film 1 is the significant amount of pimples ~1 μm^2 in size (see Figure 8). These pimples are formed when Type I cracks and small ellipsoidal cracks come into contact. These defects might be of various origin. Similar pimples are sometimes detected on Ni−W substrates.

AFM images of the surface structure of CeO_2 buffer layers annealed at 1000 °C were carried out and are

illustrated in Figures 10−13. The grain size distribution in Film 2 is uniform and reproduces the surface of the substrate (see Figure 12). Note that we are studying the area where only Type I cracks exist. The high-resolution AFM image in Figure 13 shows the globular morphology of CeO_2 films. Pores of various sizes (up to ~50 nm) can be observed. The section profile of the image along the selected line shows the maximum height difference in the sample, which is ~14 nm.

On the AFM pictures of Film 1, the surface is covered with the same net of Type II cracks that was observed via SEM (see Figure 10). Here, the CeO_2 layer consists of densely packed crystallites (see Figure 11). The section profile of the image along the selected line shows much bigger height differences in Film 1, compared to Film 2 (the maximum gradient is ~120 nm). AFM confirms that doping of CeO_2 films with La^{3+} reduces the roughness of the layer. The root-mean square (rms) roughness values on a 30 μm × 30 μm surface area for Film 1 and Film 2 are 11.3(5) and 8.4(5) nm, respectively.

4. Conclusions

The mixed-ligand complex formation approach was successfully applied for the modification of cerium(III) acetate as a precursor for metal-organic chemical surface deposition (MOCSD) of CeO_2 and $Ce(La)O_2$ buffer layers on cube-textured Ni−W tapes. Monoethanolamine (MEA) and diglyme were used as both ligands and solvents, in addition to acetate and nitrate ligands, for the preparation of metal−organic precursors. The formation of mixed-ligand Ce(IV) complexes in both liquid and gel precursor forms was confirmed by electrospray ionization mass spectroscopy (ESI MS) and ^1H nuclear magnetic resonance (NMR) spectroscopy. The advantages of the new precursor are high concentration, stability, and excellent wetting behavior toward Ni−5 at.% W substrates. Rare-earth elements can be easily incorporated into them as dopants, as was shown on an example of La^{3+}. Studies of the decomposition behavior of the precursor gels, using thermogravimetry (TG) and differential thermogravimetry (DTG) techniques, lead to a better understanding of the decomposition pathways before the crystallization in chemical surface deposition (CSD)-prepared CeO_2 film samples. The formation of polycrystalline CeO_2 is observed at 300 °C in air. Annealing at 1000 °C in an Ar/H_2 atmosphere leads to highly textured CeO_2 films. La^{3+} incorporation into the CeO_2 films significantly improves the texture and surface of the film. Further work on incorporation of other cations is currently in progress.

Acknowledgment. The authors thank Dr. A. Borisenko for NMR spectra measurements, as well as Dr. S. Samoilenkov and Dr. A. Kamenev for conducting EBSD and SEM studies of our samples. We are grateful to V. Lebedev for his help with AFM measurements, and we also are grateful to Dr. A. R. Kaul, Dr. A. Blednov, Dr. D. Villágran, and Dr. V. Amelichev for valuable discussions. This work was financially supported by RFBR (through Grant No. 08-03-01012) and the SuperOx Company (Russia).